PCCP

PAPER

View Article Online
View Journal | View Issue

Cite this: *Phys. Chem. Chem. Phys.*, 2021, **23**, 14325

$C_{14}H_{10}$ polycyclic aromatic hydrocarbon formation by acetylene addition to naphthalenyl radicals observed†

Jeehyun Yang,[a] Mica C. Smith,[b] Matthew B. Prendergast,[b] Te-Chun Chu[b] and William H. Green *[b]

The formation of polycyclic aromatic hydrocarbons (PAHs) during combustion has a substantial impact on environmental pollution and public health. The hydrogen-abstraction-acetylene-addition (HACA) mechanism is expected to be a significant source of larger PAHs containing more than two rings. In this study, the reactions of 1-naphthalenyl and 2-naphthalenyl radicals with acetylene (C_2H_2) are investigated using VUV photoionization time-of-flight mass spectrometry at 500 to 800 K, 15 to 50 torr, and reaction times up to 10 ms. Our experimental conditions allow us to probe the Bittner–Howard and modified Frenklach HACA routes, but not routes that require multiple radicals to drive the chemistry. The kinetic measurements are compared to a temperature-dependent kinetic model constructed using quantum chemistry calculations and accounting for chemical-activation and fall-off effects. We measure significant quantities of $C_{14}H_{10}$ (likely phenanthrene and anthracene), as well as 2-ethynylnaphthalene ($C_{12}H_8$), from the reaction of the 2-naphthalenyl radical with C_2H_2; these results are consistent with the predictions of the kinetic model and the HACA mechanism, but contradict a previous experimental study that indicated no $C_{14}H_{10}$ formation in the 2-naphthalenyl + C_2H_2 reaction. In the 1-naphthalenyl radical + C_2H_2 reaction system, the primary product measured is $C_{12}H_8$, consistent with the predicted formation of acenaphthylene *via* HACA. The present work provides direct experimental evidence that single-radical HACA can be an important mechanism for the formation of PAHs larger than naphthalene, validating a common assumption in combustion models.

Received 10th April 2021,
Accepted 14th June 2021

DOI: 10.1039/d1cp01565f

rsc.li/pccp

1 Introduction

The chemical mechanisms of polycyclic aromatic hydrocarbon (PAH) formation, growth, and partitioning into the particulate phase are not well understood despite their importance in accurately predicting the impact of PAHs on the environment. PAHs are molecules containing fused aromatic rings that are known to be produced in fuel-rich regions of combustion engines, industrial process streams, and interstellar media.[1] Several PAHs are also classified as mutagenic and carcinogenic substances.[2] Many experimental flame studies have linked PAHs with the formation of soot, a byproduct of combustion that decreases its efficiency and contributes to air pollution when emitted into the atmosphere.[3] PAHs are also undesirable side products in many other industrial processes. Previous theoretical calculations have helped elucidate some of the complex chemistry involved, identifying several key mechanisms that are likely to be significant under combustion-relevant conditions.[4–6]

A prevailing mechanism that rationalizes the formation of larger PAHs from 1- and 2-ringed aromatics is the hydrogen-abstraction-acetylene-addition (HACA) mechanism: an aromatic radical formed *via* hydrogen abstraction adds to acetylene (C_2H_2) to form a larger vinylic radical adduct.[3,7–9] HACA can proceed *via* several different routes. The vinylic radical can add sequentially to another C_2H_2 to produce a larger conjugated intermediate for which ring closure is possible, or the vinylic radical can isomerize (*e.g.* to form a vinyl-substituted aryl radical), and then that isomer can add the second C_2H_2. At higher temperatures, the vinylic radical adduct rapidly undergoes H-atom loss to form an ethynyl-substituted aromatic species, which can undergo HACA again (by attack by a second H atom) to add a second C_2H_2 molecule. While a wealth of evidence exists from both indirect flame experiments and theoretical calculations linking the HACA mechanisms to PAH growth, few experimental studies

[a] *Department of Earth, Atmospheric and Planetary Sciences, Massachusetts Institute of Technology, Cambridge, MA 02139, USA*
[b] *Department of Chemical Engineering, Massachusetts Institute of Technology, Cambridge, MA 02139, USA. E-mail: whgreen@mit.edu*

† Electronic supplementary information (ESI) available. See DOI: 10.1039/d1cp01565f

have directly investigated the chemical kinetics of HACA.[3,4,10] The chemistry of radical species derived from the simplest six-membered aromatic hydrocarbon, benzene, has previously been investigated using quadrupole mass spectrometry and cavity ringdown spectroscopy to measure the temperature-dependent rate of the reaction of phenyl radicals with C_2H_2.[11–13] Recent investigations using photoionization mass spectrometry to probe phenyl radical (C_6H_5) reactions with C_2H_2 in the 500–800 K range have revealed an ion signal with a mass-to-charge ratio of 128 (m/z = 128) consistent with naphthalene, which is rationalized *via* the HACA mechanism with sequential H-atom loss and C_2H_2 addition.[14,15]

Combustion models commonly assume that naphthalene ($C_{10}H_8$), the simplest PAH, follows the HACA mechanism, in a manner similar to benzene, to form larger three-ring PAHs, an assumption that is corroborated by theoretical calculations.[4,16] Hydrogen abstraction from naphthalene produces two distinct $C_{10}H_7$ radicals: 1-naphthalenyl and 2-naphthalenyl radicals. Sequential addition of C_2H_2 to these radicals can lead to different products. Theoretical investigations indicate that 1-naphthalenyl radical reactions with C_2H_2 preferentially form acenaphthylene ($C_{12}H_8$) *via* a $C_{12}H_9$ intermediate with a five-membered ring. On the other hand, the reaction of 2-naphthalenyl with C_2H_2 is expected to produce a vinylic adduct that can live long enough to undergo intramolecular hydrogen transfer followed by addition to a second C_2H_2 molecule and ring-closing to form either phenanthrene or anthracene ($C_{14}H_{10}$).[4,10] These pathways of ''two-to-three-ring'' PAH growth compete with the β-scission pathways leading to loss of a hydrogen atom and formation of ethynylnaphthalene. At combustion temperatures and pressures, theory predicts acenaphthylene and ethynylnaphthalene isomers to be the major stable products of the naphthalene HACA mechanism,.[4] But at lower temperatures the Bittner–Howard[9] and modified Frenklach pathways[17,18] are predicted to be significant for 2-naphthalenyl radical, leading to formation of significant amounts of phenanthrene and anthracene. (Both of these stable $C_{14}H_{10}$ species are commonly observed in flames.)

Only a few experimental investigations have been conducted to test these theoretical predictions. The reaction of 1-naphthalenyl + C_2H_2 was investigated in a shock tube experiment at temperatures above 950 K,[19] and the kinetics of the 2-naphthalenyl + C_2H_2 reaction was measured using cavity ring-down spectroscopy following laser photolysis of bromonaphthalene at 303 to 448 K.[20] The temperature-dependent rate coefficients for these reactions were in agreement with theoretical predictions.[19,20] A product detection study for 1-naphthalenyl and 2-naphthalenyl reactions with C_2H_2 was recently conducted at temperatures up to 1500 K using mass spectrometry to monitor products formed in a silicon carbide micro-reactor.[21] Both radical isomer reactions led to products at m/z = 152, corresponding to acenaphthylene or ethynylnaphthalene, but surprisingly, no product formation at m/z = 178 corresponding to phenanthrene or anthracene, was observed.[21]

Recent theoretical calculations have been reported suggesting that addition of acetylene to 2-naphthalenyl radical at temperatures around 800 K will lead to formation of phenanthrene and anthracene.[22] At around 800 K, the formation and branching of major stable products (including phenanthrene, anthracene, acenaphthylene, and ethynylnaphthalene) are expected to be highly sensitive to temperature. In order to reconcile previous investigations of the reaction mechanisms for growth from naphthalenyl radicals to three-ring species, direct experimental measurements of the time-resolved product distributions are needed.

In the current work, we perform direct measurements of the 1-naphthalenyl and 2-naphthalenyl radical reactions with C_2H_2 to test the validity of a kinetic model recently developed within our group.[22] Vacuum-ultraviolet photoionization time-of-flight mass spectrometry (VUV-PI-TOF-MS) is used to measure the time-dependent product formation at 500 to 800 K and 15 to 50 torr. Products from the first and second C_2H_2 addition are observed and the results compared with the kinetic model from Chu *et al.*[22] Potential explanations for the observed kinetic behavior are discussed.

2 Experimental

For both the 1- and 2-naphthalenyl + C_2H_2 reactions, experiments were conducted at temperatures between 500 K and 800 K and total gas pressures between 15 torr and 50 torr. Experiments were carried out in a vacuum ultraviolet photoionization time-of-flight mass spectrometry (VUV-PI-TOF-MS) apparatus previously described in literature[23,24] and only briefly described here. The apparatus features a bow-tie shaped quartz flow reactor enclosed in a stainless steel high-vacuum chamber (pressure: 10^{-5}–10^{-8} torr) equipped with two quartz windows to allow laser access for photolysis of the radical precursor. The reactor includes two wide outer sections (inner diameter = 36 mm; length = 295 mm each) and a narrower middle section (inner diameter = 16 mm; length = 400 mm). The wider sections of the reactor enable measurements with laser absorption spectroscopy, which has been used in some studies; however, the present work only focuses on VUV-PI-TOF-MS. A pinhole (diameter = 300 ± 25 μm) was laser drilled into the middle section of the reactor to allow the escape of gases from the reactor into the high-vacuum chamber.[6] A skimmer was used to sample the gas passing through the pinhole, producing a supersonic molecular beam containing the gas-phase species, which then underwent photoionization. The cations produced are detected by reflectron time-of-flight mass spectrometry.

The radical precursors 1-iodonaphthalene (obtained from Sigma Aldrich, 97% purity) and 2-iodonaphthalene (obtained from Oakwood Chemicals, >98% purity) were degassed with several freeze–pump–thaw cycles using liquid nitrogen. Samples of 1-iodonaphthalene and 2-iodonaphthalene were analyzed by proton NMR to assess potential contamination by the opposing isomer. No significant peak of opposing isomer was found from each precursor, and it is reasonable to conclude that opposing isomer contamination is less than 0.5% (The H-NMR analysis can be found in Fig. S1 and S2 in the ESI†). Control experiments were also performed using

1-bromonaphthalene (Sigma Aldrich, 97% purity) and 2-bromonaphthalene (Sigma Aldrich, 97% purity) instead of each corresponding iodonaphthalene.

Throughout each experiment, a mixture of radical precursor (usually 1- or 2-iodonaphthalene), excess C_2H_2 (Airgas, $\geq$99.5%), and helium bath gas (Airgas, >99.999%) flowed continuously through the reactor. The gas mixture was created by bubbling a stream of helium with a backing pressure of 10 psig through the liquid iodonaphthalene in a heated bubbler at 70 °C. The resulting gas stream was then combined with the C_2H_2 stream (that was passed through an activated carbon filter to remove residual acetone) and a small flow of helium containing seven calibration gases (obtained from Airgas: propylene, 80.00 ppm; 1,3-butadiene, 97.27 ppm; benzene, 88.00 ppm; furan, 97.52 ppm; cyclohexane, 100.2 ppm; toluene, 80.00 ppm; and *n*-heptane, 99.97 ppm; analytical uncertainty ±2%) used to calibrate the time-of-flight mass spectrometer response.[23] The pressure inside the reactor was controlled by a butterfly valve on the reactor outlet to a Roots type blower (Leybold). Flow rates were controlled using mass flow controllers (MKS Instruments, USA). The lines between the bubbler and the reactor inlet were heated to >70 °C to prevent condensation. The total flow rate was adjusted during experiments so the gas in the reactor was completely refreshed every 1 s. The quartz reactor was heated to temperatures from 500 to 800 K with Nichrome ribbon wire wrapped around the exterior of the tube. Two K-type thermocouples inside the reactor were used to control the experimental temperature. The gas temperature profile throughout the length of the reactor was characterized prior to experiments with a thermocouple extended inside the reactor, and found to be constant within ±2% (2 standard deviations) in the main sampling region (center ±5 cm).

In each experiment, a pulsed 266 nm Nd:YAG laser (Spectra-Physics Quanta-Ray, fourth harmonic) with a repetition rate of approximately 1 Hz was directed co-axially along the reactor to generate 1- or 2-naphthalenyl radicals from the radical precursor in the flowing gas mixture, initiating the radical chemistry. The reaction products were monitored using VUV-PI-TOF-MS to probe the molecular beam of gas sampled from the reactor as mentioned above. The VUV ionizing radiation was produced by a pulsed 355 nm Nd:YAG laser (Quantel Brilliant, third harmonic) focused into a stainless steel cell containing 90 torr of Xe : Ar (1 : 10) gas.[25,26] The resulting 118.2 nm (10.49 eV) light was directed through an off-axis MgF_2 lens through a small hole to physically separate the VUV radiation from the remaining 355 nm light.[25,27] The VUV beam then intersected with the molecular beam of sampled gas, producing ions that were collected and focused into a reflectron time-of-flight mass spectrometer (Kore Technology). The resulting mass spectrum was averaged over 150 photolysis laser shots, and the peak at each m/z of interest was integrated to obtain the signal intensity. Changes in signal intensity with reaction time were measured by varying the time delay between the photolysis laser pulse and the VUV photoionization laser pulse. Several spectra were also collected before the photolysis pulse for a background subtraction, so changes in 266 nm laser dependent signal can be analyzed for kinetic information. Additional corrections were made for signals originating from the natural abundance of ^{13}C; assuming that m/z = 152 signal entirely originated from $C_{12}H_8$ and there was no iodo compounds interference by HCCI and C_2H_2I. In the case of the m/z = 153 signal, which was attributed to both $C_{12}H_9$ radicals and the ^{13}C isotopologue of $C_{12}H_8$ (the mass spectrometer resolution was not high enough to distinguish these two species), the processed signal intensity for $C_{12}H_9$ ($S^{expt}_{m/z=153}$) reported in the figures here was calculated as

$$S^{expt}_{m/z=153} = S^{expt}_{raw,m/z=153} - S^{expt}_{raw,m/z=152} \times 12 \times \frac{1.1\%}{98.9\%} \quad (1)$$

where $S^{expt}_{raw,m/z=153}$ and $S^{expt}_{raw,m/z=152}$ are the raw signal intensities of the m/z = 153 and 152 ions, respectively. The multiplicative terms account for the relative abundance of the ^{13}C isotopologue (^{13}C natural abundance is 1.1% for each of the 12 carbon atoms). An analogous calculation was used to correct the $C_{12}H_{10}$ signal for $^{13}CC_{11}H_9$ and $^{13}C_2C_{10}H_8$ at m/z = 154, and the $C_{14}H_{11}$ signal for $^{13}CC_{13}H_{10}$ at m/z = 179 (assuming that m/z = 178 signal is 100% $C_{14}H_{10}$) as below.

$$S^{expt}_{m/z=154} = S^{expt}_{raw,m/z=154} - S^{expt}_{m/z=153} \times 12 \times \frac{1.1\%}{98.9\%} - S^{expt}_{raw,m/z=152} \times 66 \times \left(\frac{1.1\%}{98.9\%}\right)^2 \quad (2)$$

$$S^{expt}_{m/z=179} = S^{expt}_{raw,m/z=179} - S^{expt}_{m/z=178} \times 14 \times \frac{1.1\%}{98.9\%} \quad (3)$$

The mass spectrometric signal intensities corresponding to the calibration gases were recorded and were found to be constant over the reaction time studied apart from the benzene signal at m/z = 78 that overlaps with products formed during the reaction (standard deviation $\leq$5.05%); experiments were performed with and without the calibration mixture to confirm its insignificant effect on the $C_{10}H_7 + C_2H_2$ reaction system. The calibration gas signals were averaged over all delay times and the response factor (R_i) for the time-of-flight mass spectrometer was determined using their VUV photoionization cross sections at 10.49 eV (listed in ESI†) and known concentrations.[23] R_i values at each m/z (excluding one outlier for propylene, as well as the R_i value for m/z = 78 that contained interference from side reactions) were averaged to obtain the average response factor R. This response factor was used to determine expected integrated mass signals for reaction products predicted from the kinetic model, as described in the following section.

An unexpectedly large m/z = 154 signal (bigger than expected from the ^{13}C satellite) was formed in the 2-iodonaphthalene + C_2H_2 experiments indicating the expected $C_{12}H_9$ (m/z = 153) product was picking up an H atom from an unknown source. Removing the C_2H_2 revealed the same sort of thing: in addition to the expected m/z = 127 signals from $C_{10}H_7$ and from I atom, an unexpectedly large signal was seen at m/z = 128 suggesting $C_{10}H_8$ formation. From these observations and several control experiments, we are confident that a reaction happened inside the pinhole in the reactor wall leading to the mass spectrometer

(see Fig. S3 and the discussion in the ESI†). In prior work by Buras *et al.*,[24] a similar phenomenon was observed when phenyl iodide was photolyzed: not just C_6H_5 (m/z = 77) was formed, but also an unexpectedly large amount of m/z = 78 suggesting the phenyl radical was picking up an H atom somewhere. The excess m/z = 154 signal tracks the computed concentration of $C_{12}H_9$. We hypothesize that some fraction of the very reactive aryl and vinylic radicals being sampled abstract H atoms in a wall reaction occurring at or inside the pinhole, so this is an artefact of our reactor sampling system. This is discussed further below.

3 Kinetic modeling

To model experimentally measured reaction rates and product branching ratios, we constructed an elementary-step reaction mechanism containing the reactions involved in the 1-naphthalenyl + C_2H_2 and 2-naphthalenyl + C_2H_2 systems recently computed at the G3(MP2,CC) level of theory by Chu *et al.*[22] This model chemistry included several new species and pathways in addition to the previously reported potential energy surface from Kislov *et al.*[4] An accurate model for the present experiments required inclusion of several side reactions not discussed by Chu *et al.* or Kislov *et al.*, but fortunately values for many of the rate coefficients of the side reactions (involving *e.g.* vinyl radicals and iodine atoms) were presented previously in the literature.[19,28,29]

The full reaction mechanism with rate coefficients and thermochemical parameters and their sources is given in CHEMKIN format in the ESI.† A few of the rate coefficients were newly-estimated in this present work, see Table S1 in the ESI.† We simulated the experiments modeling the reactor as isobaric, isothermal, and well-mixed (homogeneous), using the model simulator included in the Reaction Mechanism Generator (RMG) suite package.[30] Sensitivity analysis was done using the Reaction Mechanism Generator (RMG) suite package.[30] Rate of Production analysis (ROP) was done using the Reaction Mechanism Simulator (RMS).[31]

In our apparatus the mass spec signals did not show perfectly sharp changes when the time delay between the photolysis and photoionization laser pulses was varied, but instead had a finite rise time of several hundred microseconds. As discussed by Middaugh *et al.*[23] this was due to several factors, most importantly diffusion of molecules across the thin gap between the photolyzed region and the pinhole, and also velocity dispersion in the pinhole and in the molecular beam. Following Middaugh *et al.* we modeled this by including a first-order sampling rate. This sampling rate was fitted to the experimentally observed rise time of the m/z = 127 signal, which was predominantly due to I atoms formed on a nanosecond timescale by the photolysis pulse. The inferred sampling rate (k_s) from the fits varied from 1200–1800 s^{-1}. There was slightly higher uncertainty in the sampling analysis for this system than in previous experiments made using this apparatus, because there were some other species contributing to the m/z = 127 signal in the mass spectra, most importantly $C_{10}H_7$. This was discussed in detail in the ESI.†

The chemical kinetics of this low-temperature system mostly follows the Bittner–Howard[9] and modified Frenklach routes.[17,18] Different from the Frenklach route that is important in high-temperature systems,[7,8,32] these lower-temperature routes only require one radical that can add first one and then a second C_2H_2 to form larger PAHs, so reaction rates of the low-temperature routes are first order in radical concentration. However, in the experiments there are some second-order disproportionations and recombination reactions that noticeably affect the measurements. In order to account for the second-order reactions in the simulations, one needs an estimate of the absolute radical concentration formed by the photolysis flash. We obtained that value from the amplitude of the m/z = 127 signal, using the known photoionization cross-section of I atom and various calibrations. The uncertainty in this estimate of the initial radical concentration, due in part to other species contributing to the m/z = 127 signal, and also due to the reactions of I atom, was discussed in the ESI† (Fig. S4). Because the second-order reactions are much slower than the first-order reactions at the reaction conditions of interest, this uncertainty in the absolute radical concentration does not affect the main findings of this work.

The resulting model predicted time-dependent concentration of each species j (with molecular weight $m/z = i$), $C_j^{\text{model}}(t)$, were summed over and converted to a value that can be compared to the experimentally measured and processed ion signal intensity at $m/z = i$ ($S_i^{\text{expt}}(t)$) using eqn (4)

$$\frac{dS_i^{\text{model}}(t)}{dt} = k_s\left[R\sum_j \sigma_j C_j^{\text{model}}(t) - S_i^{\text{model}}(t)\right] \quad (4)$$

where σ_j is the VUV photoionization cross-section (PICS) for each species j at 10.49 eV (listed in Table 1), and R is the response factor for our apparatus described in the Experimental section.

We can classify radicals into resonance-stabilized radicals and non-resonance-stabilized radicals. Resonance-stabilized radicals (RSR) are free radicals that are stabilized by delocalizaion (resonance). The benzyl radical (C_7H_7) is one example. Non-resonance-stabilized radicals are those where in all the important Lewis structures the radical remains on the same atom, *i.e.* the SOMO is not conjugated with a π system or free electron pair or empty valence orbital. The phenyl radical

Table 1 Photoionization cross-sections (PICS) used in this study

m/z	Species	PICS (Mb)	2σ Uncertainty (Mb)	Ref.
152	Acenaphthylene	54	±27[a]	36
152	(1-,2-)Ethynylnapthalene	54	±27[a]	36
153	$C_{12}H_9$ RSR species	24	±12[a]	36[b]
153	$C_{12}H_9$ non-RSR species	5	±3[a]	33[c]
154	(1-,2-)Vinylnaphthalene	61	±31[a]	36
154	C_2H_3I	50	±15	28[d]
178	Phenanthrene	30	±15[a]	37 and 38
178	Anthracene	31	±16[a]	37 and 38

[a] Assumed with a 50% uncertainty. [b] Assumed to have the same PICS as 2,3-dihydro-2-naphthalenyl radical. [c] Assumed to have the same PICS as 2-propenyl radical. [d] Assumed to have the same PICS as C_4H_5I.

(C_6H_5) is one example of a non-resonance-stabilized radical: although there is a lot of resonance in the π system of phenyl, the SOMO is in the plane of the ring, orthogonal to the π orbitals, so it is not conjugated. For $C_{12}H_9$ non-resonance-stabilized radicals (non-RSR), their PICS were assumed to be same as that of 2-propenyl radical that is also a non-RSR: 5 Mb.[33] Radicals that have one electron in their HOMO are expected to have lower PICS than closed-shell molecules that have two electrons in their HOMO since the electron is ejected from lower occupancy. For example, Xu and Pratt's model expects the PICS of radical species to be half that of the analogous closed-shell species.[34] However, aromatic (RSR) have been observed to have higher PICS compared to non-RSR, *e.g.* the benzyl radical PICS = 25.5 Mb.[35] For this reason, $C_{12}H_9$ RSR PICS were assumed to be the same as that of 2,3-dihydro-2-naphthalenyl radical (24 Mb), which is also a RSR.[36]

The amplitude of the integrated mass signals measured in the experiment can vary daily with the reactor alignment, the laser pulse energies, and other instrument parameters. In order to correct for these variations, the experimentally observed integrated mass signals for each m/z were normalized to the experimentally observed integrated mass signals at m/z = 127 (mainly I atom) recorded at the time after photolysis when the m/z = 127 integrated mass signal reached its peak. This normalizing process was based on the assumption that the peak intensity was unchanged throughout each experimental set (*i.e.* different delay times but otherwise same experimental conditions, measured on the same day). These normalized integrated MS signals were compared with model-predicted integrated MS signals that also were normalized to those of model-predicted I-atom signal intensity, *i.e.* we are comparing predicted and experimental product yields per radical introduced. This procedure not only corrects for experimental variations, but also removes the uncertainty in the response factor R.

4 Results and discussion

4.1 Time-of-flight mass spectrometry

The 1- and 2-naphthalenyl radicals ($C_{10}H_7$, m/z = 127) are generated within the flow reactor by photolysis of 1-iodonaphthalene ($C_{10}H_7I$, m/z = 254), and separately 2-iodonaphthalene, and react with excess C_2H_2 to form products detected by VUV-PI-TOF-MS (PI energy = 10.49 eV). Fig. 1 shows representative mass spectra acquired after photolysis of the iodinated radical precursors in the presence of (C_2H_2).

The m/z = 152 ion signal shown in Fig. 1 is attributed to $C_{12}H_8$ isomers following C_2H_2 addition to naphthalenyl radicals and subsequent H-atom loss. The m/z = 153 signal is assigned to the $C_{10}H_7$ + C_2H_2 adduct ($C_{12}H_9$) isomers and the ^{13}C isotopologues of $C_{12}H_8$. The m/z = 178 raw signals are due to $C_{14}H_{10}$ isomers and can be rationalized by a HACA mechanism with a total of two C_2H_2 additions.

Ion signals with m/z = 42, 54, 68, 84, 92, and 100 correspond to the calibration mixture described in the Experimental section and do not exhibit a noticeable change in signal intensity with reaction time (*i.e.* delay between photolysis and photoionization lasers).

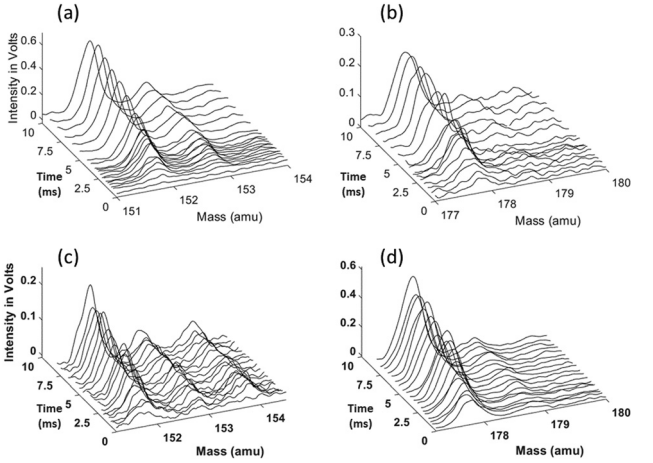

Fig. 1 Representative time-of-flight mass spectra at various peaks of interest (m/z = 152, 153, and 178) at various delay times for 1-naphthalenyl + C_2H_2 (top: a and b) and 2-naphthalenyl + C_2H_2 (bottom: c and d) systems. Reaction conditions: (a) and (b) 800 K, 25 torr, $[C_2H_2]$ = 3.0 × 10^{16} molecules per cm^3, 1-naphthalenyl concentration $[C_{10}H_7]_0$ = 4.2 × 10^{11} molecules per cm^3; (c) and (d) 700 K, 15 torr, $[C_2H_2]$ = 3.0 × 10^{16} molecules per cm^3, 2-naphthalenyl concentration $[C_{10}H_7]_0$ = 3.0 × 10^{11} molecules per cm^3.

Time-dependent signals at m/z = 52 (C_4H_4), 53 (C_4H_5), 78 (C_6H_6), and 79 (C_6H_7) are likely the result of side reactions detailed by Smith *et al.*[28] Time-dependent signals at m/z = 126, 128, 154, 179, and 180 were also measured. The small signal at m/z = 126 rises immediately after photolysis, suggesting either $C_{10}H_6^+$ is formed by dissociative ionization of the $C_{10}H_7$ after photolysis of $C_{10}H_7I$, or a minor photolysis mechanism forming naphthyne ($C_{10}H_6$) followed by its photoionization. The signal at m/z = 128 can be attributed to several sources: (i) the ^{13}C isotopologue of $C_{10}H_7$, (ii) naphthalene ($C_{10}H_8$), and (iii) hydrogen iodide (HI). The m/z = 154 signal can be attributed to $^{13}CC_{11}H_9$, $^{13}C_2C_{10}H_8$, $C_{12}H_{10}$, and plausibly C_2H_3I from C_2H_3 + I recombination (after C_2H_2 + H).[28] The m/z = 179 signal is attributed to the convolution of the $^{13}CC_{13}H_{10}$ isotopologue of the $C_{14}H_{10}$ products and the $^{13}CC_3H_3I$ isotopologue of the C_4H_3I products. The observed m/z = 180 signal is predominantly attributed to C_4H_5I from C_4H_5 + I, and also partially to vinyl radical (C_2H_3) recombination with the $C_{12}H_9$ radicals. Since the formation of $C_{14}H_{11}$ is predicted to be minor based on the model prediction, the contribution to this signal from $C_{14}H_{11}$ + H should be negligible.

All the major reaction products observed in the mass spectra (Fig. 1) are predicted by the model for both the 1-naphthalenyl + C_2H_2 and 2-naphthalenyl + C_2H_2 reaction systems, except for the signal at m/z = 178 observed from 1-naphthalenyl + C_2H_2. These observed mass spectra and the predictions of the kinetic model are explained further in the following sections.

4.2 Naphthalenyl + acetylene reaction kinetics

4.2.1 1-Naphthalenyl + acetylene. The normalized time-dependent integrated mass-to-charge (m/z) signal intensities

from the reaction of 1-naphthalenyl radical with C_2H_2 at 500 K and 25 torr, 700 K and 25 torr, and 800 K and 25 torr are shown in Fig. 2a–c. Signals were detected at m/z = 152 and 153 under all experimental conditions and a significant additional signal at m/z = 178 was observed at temperatures $\geq$700 K. This m/z = 178 signal will be discussed later. The experimental results are compared with the model prediction up to 10 ms after the photolysis pulse as shown in Fig. 2a–c. Scheme 1 shows a part of the $C_{12}H_9$ potential energy surface from Chu *et al.*[22] The model predicted primary reaction pathway for acetylene addition to 1-naphthalenyl radical is colored red in Scheme 1. Multiple stable products may be formed, including acenaphthylene (ACN), 1-ethynylnaphthalene (ETN-1), and others not included in Scheme 1 but included in the full model (see ref. 22). According to the model, between 500 K and 800 K, the m/z = 152 signal is computed to be mostly acenaphthylene ($C_{12}H_8$) as shown in Fig. 2. The model predicted behavior of the signal at m/z = 153 is mostly determined not by the initial adduct, but by the very stable intermediate isomer N8-1 (see Scheme 1; isomers were named using the nomenclature in Kislov *et al.*[4]) as shown in Fig. 2.

The model predicts an increasing product branching ratio of acenaphthylene (m/z = 152) to N8-1 (m/z = 153) with increasing temperature, consistent with the experimental data shown in Fig. 2d–f. This behavior is attributed to the increased rate of well-skipping reaction at higher temperatures (1-naphthalenyl radical + C_2H_2 → ACN + H, shown in Scheme 1), which favors ACN formation over N8-1 formation. At every set temperature condition, the initial steep increase of ACN observed in the experiments up until 2 ms (Fig. 2a–c) is attributed to rapid well-skipping reactions as assessed by the Rate Of Production (ROP) analysis shown in Fig. S12 (ESI†), up to 0.5 ms. This steep increase is followed by relatively slow formation of acenaphthylene through disproportionation reactions (N8-1 + I → ACN + HI). At 700 K, the steep increase is followed by relatively flat line, which indicates no significant acenaphthylene formation after the well-skipping reaction is exhausted (due to consumption of the initial $C_{10}H_7$ radical). At 800 K, the steep increase due to well-skipping reaction is followed by gradual increase due to disproportionation with I atom (N8-1 + I → ACN + HI). The switch in mechanism is easy to see in Fig. 2f where the product branching ratio of m/z = 152 to 153 stays relatively flat up until 2 ms and then gradually increases after 2 ms as the disproportionation reaction becomes more important than the well-skipping reaction of the initial reactants $C_{10}H_7$ + C_2H_2.

The pressure dependence of the observed and predicted 1-naphthalenyl + C_2H_2 product branching ratio was investigated at 25 and 50 torr. As shown in Fig. 3, up until 2 ms, the observed

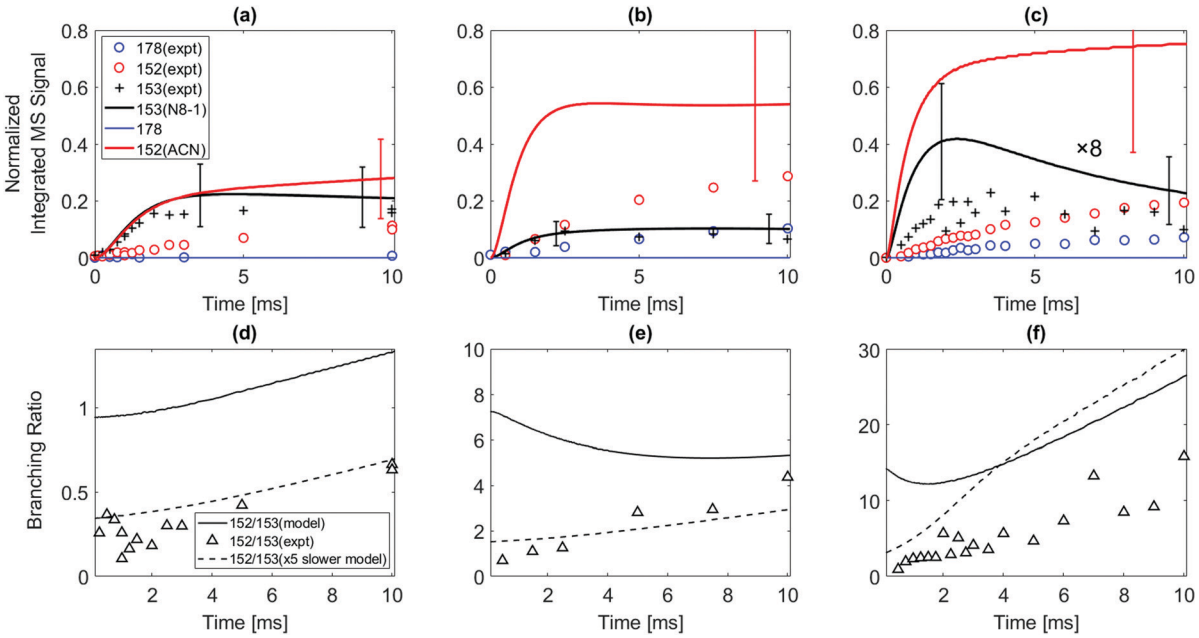

Fig. 2 (Top) Normalized time-dependent integrated m/z signals measured up to 10 ms after the photolysis of the 1-iodonaphthalene in the presence of C_2H_2. Red open circles indicate the m/z = 152 signal; blue open circles indicate m/z = 178 signal; and the black cross symbols (+) indicate the ^{13}C-corrected m/z = 153 signal from the experiment. Solid lines are the model predictions. Red: m/z = 152 (mostly acenaphthylene); black: m/z = 153 (mostly N8-1). The model does not predict significant production of m/z = 178 (apparently $C_{14}H_{10}$) at these conditions. In (c), the black solid line (including its error bars) and black cross symbols are multiplied by 8 for scale. Uncertainty ranges of the model predictions (due to uncertainties in PICS) are shown as error bars. (Bottom) The branching ratio of m/z = 152 to m/z = 153. Black open triangle symbols indicate the experimentally observed ratio of m/z = 152 to m/z = 153; black solid line indicates model predicted ratio of m/z = 152 to m/z = 153; black dashed line indicates model predicted ratio of m/z = 152 to m/z = 153 when the computed k for the well-skipping reaction of 1-naphthalenyl radical + C_2H_2 to form acenaphthylene was reduced by a factor of 5. Reactor conditions: (a) and (d) 500 K, 25 torr, initial radical concentration $[C_{10}H_7]_0$ = 2.4 × 10^{11} molecules per cm^3; (b) and (e) 700 K, 25 torr, $[C_{10}H_7]_0$ = 1.5 × 10^{11} molecules per cm^3; (c) and (f) 800 K, 25 torr, $[C_{10}H_7]_0$ = 4.2 × 10^{11} molecules per cm^3. The concentration of C_2H_2 for all the experiments was 3 × 10^{16} molecules per cm^3.

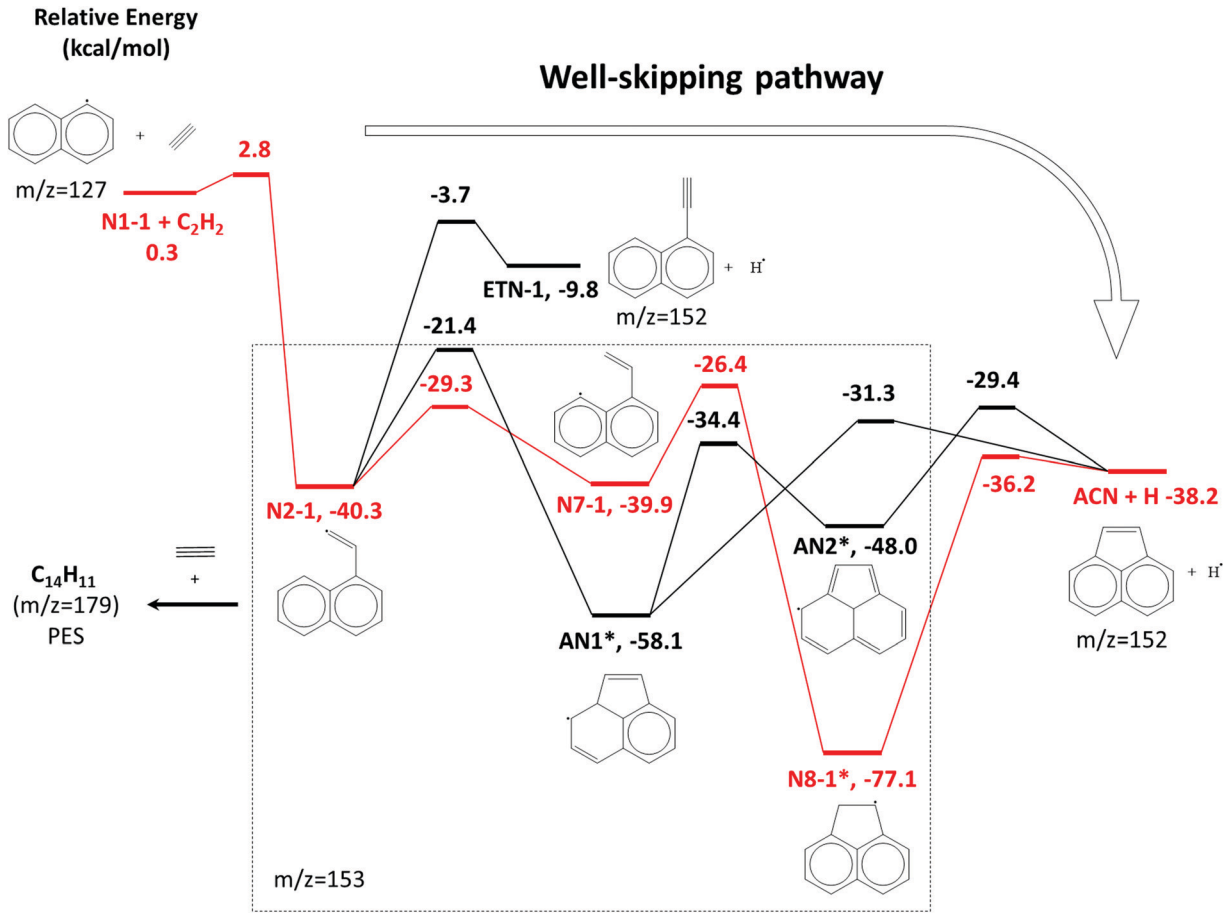

Scheme 1 A part of the $C_{12}H_9$ potential energy scheme from Chu *et al.*[22] The primary reaction pathway for 1-naphthalenyl + C_2H_2 predicted by the kinetic model under the experimental conditions in this work is shown in red lines. The asterisks indicate $C_{12}H_9$ RSR species.

product branching ratio of m/z = 153 to 152 increases from 25 to 50 torr. This behavior might be attributed to increased collisional stabilization into m/z = 153 product well (predominantly N8-1) at higher pressure, which decreases the probability of well-skipping to acenaphthylene product. The m/z = 153 radical then slowly dissociates to yield m/z = 152 on a longer time scale. However, the observed pressure dependence is not as strong as predicted by the model. Discrepancies between the model and the experimental data will be discussed in a later section.

4.2.2 2-Naphthalenyl + acetylene. As seen in Scheme 2, the reaction of 2-naphthalenyl radical with C_2H_2, unlike acetylene addition to 1-naphthalenyl radical, is predicted to easily proceed *via* sequential C_2H_2 addition steps under the experimental conditions in this work. Multiple stable products may be formed, including 2-ethynylnaphthalene (ETN-2; m/z = 152) and the three-ring PAHs anthracene and phenanthrene (m/z = 178). Fig. 4 shows normalized time-dependent species integrated mass signals measured for the reaction of 2-naphthalenyl with C_2H_2 under various experimental conditions compared with corresponding model prediction.

The model predicts most of the m/z = 152 signal observed when 2-naphthalenyl reacts with acetylene is due to 2-ethynylnaphthalene. According to ROP analysis (see Fig. S13, ESI†), at the conditions of these experiments, up until 600 K, the formation of m/z = 152 (2-ethynylnaphthalene) is predominantly due to disproportionation between I atom and the radical adduct, N2-2 (*i.e.* N2-2 + I → 2-ethynylnaphthalene + HI). However, it has to be noted that this I atom involved reaction is estimated. Without this disproportionation reaction with I atom, the model predicts formation of m/z = 152 at temperatures $\lesssim$600 K would be negligible. The formation of 2-ethynylnaphthalene is not sensitive to disproportionation above 700 K. As in the case of 1-naphthalenyl + C_2H_2, an initial sharp increase followed by slow increase in m/z = 152 formation can be observed in the model prediction for the 2-naphthalenyl + C_2H_2 system above 700 K. According to ROP analysis in Fig. S13 (ESI†), above 700 K most of the 2-ethynylnaphthalene product observed is due to β-scission of the initial adduct (N2-2). At the very shortest times, before much N2-2 has accumulated, the direct chemically activated pathway is also important.

In the model prediction, most of the m/z = 178 product is phenanthrene and anthracene (with a predicted branching ratio of 2 : 1 at 500 K and 1 : 1 at higher T). At all the conditions of the present experiments, the ROP analysis (see Fig. S15 and S16 of ESI†) shows that the formation of m/z = 178 is predominantly due to second acetylene additions to N2-2, N8-2, and N11-2 directly forming m/z = 178 plus H atom; see Scheme 2. Phenanthrene formation in the model is predominantly determined by

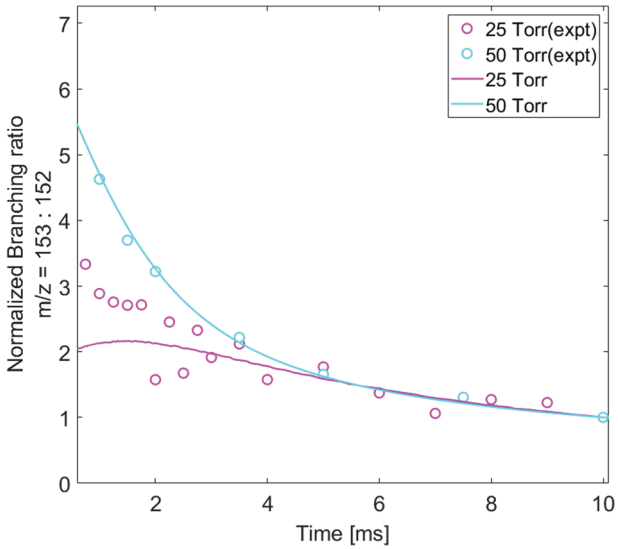

Fig. 3 The time-dependent ratio of isotope-corrected m/z = 153 to m/z = 152 signals, both normalized to their intensities at 10 ms to remove the effect of different PICS. At short times radicals (m/z = 153) are formed from the addition $C_{10}H_7$ + C_2H_2, but those radicals then lose an H to form m/z = 152 (primarily acenaphthylene according to the model). Open circle symbols indicate the experimentally observed and then normalized branching ratio of m/z = 153 to m/z = 152 under each experimental condition (magenta: 800 K, 25 torr, and cyan: 800 K, 50 torr); Solid lines indicate model predicted and then normalized branching ratio of m/z = 153 to m/z = 152 under each experimental condition (magenta: 800 K, 25 torr, and cyan: 800 K, 50 torr).

N2-2 + acetylene well-skipping reaction at every temperature. Anthracene formation is mostly attributed to N2-2 + acetylene well-skipping reaction up to 600 K, but at temperatures above 700 K, N11-2 + acetylene well-skipping reaction becomes more important for Anthracene formation. In the model prediction, for temperatures $\geq$700 K, most of radical adducts (*i.e.* N2-2, N8-2, and N11-2) are consumed within 3 ms, leading to the flattening in the profiles (Fig. 4c and d).

When the temperature increases from 500 to 600 K, the model predicts that the product branching ratio of m/z = 152 to m/z = 178 decreases as shown in Fig. 4e and f. This behavior is due to increased rate of well-skipping reaction to form three-ring PAHs (*i.e.* phenanthrene and anthracene). (At these low temperatures, the main pathway to m/z = 152 is radical disproportionation with I atom, which is much less sensitive to temperature.) However, from 700 to 800 K, when the temperature is high enough for significant β-scission of N2-2, the model predicts that the branching ratio shifts to favor m/z = 152 formation over m/z = 178 as shown in Fig. 4g and h. At high temperatures, the three radical adducts N2-2, N8-2, and N11-2 rapidly interconvert, so they are partially equilibrated. As the temperature increases, fewer of these radical adducts are collisionally stabilized, and also the β-scission of thermalized N2-2 to m/z = 152 + H becomes more important. This explains why the yield of m/z = 178 drops in the model (and less dramatically in the experimental data) as temperature increases from 700 K to 800 K, Fig. 4. Different acetylene concentration was also tested as shown in Fig. 4f. While maintaining all the other experimental condition same, only acetylene concentration was reduced from 3 × 10^{16} molecules per cm^3 to 1 × 10^{16} molecules per cm^3 compensating with additional helium. As expected from the model prediction, this results in increased branching ratio of m/z = 152 to m/z = 178 due to decreased rate of second acetylene addition to m/z = 153 (forming m/z = 178). The experimental data (black triangles) show reasonable agreement with the model prediction (solid black line).

While the m/z = 153 signal from 1-naphthalenyl radical + C_2H_2 is mostly predicted in the model to be resonance stabilized radical, N8-1, under every experimental condition in this study, there are at least six different $C_{12}H_9$ isomers predicted from the model of 2-naphthalenyl radical + C_2H_2, as shown in Fig. 5. As discussed further in later section, these model predicted $C_{12}H_9$ isomers can be categorized into two different species types: non-resonance stabilized radicals (non-RSR) and resonance stabilized radicals (RSR). As shown in Fig. 5a, the model suggests initial formation of $C_{12}H_9$ non-RSR species (N2-2, N8-2, and N11-2), followed by the appearance of $C_{12}H_9$ RSR species (N17-2, N16-2, and N14-2). When $C_{12}H_9$ non-RSR species are formed, these species go through various reactions depending on the temperature conditions: (i) disproportionation reaction with I atom, (ii) isomerization into $C_{12}H_9$ RSR species, (iii) second acetylene addition to form anthracene or phenanthrene, and (iv) β-scission reaction to form 2-ethynylnaphthalene. When the temperature is lower than 600 K, (i) and (iii) are dominant in the system. However, at temperatures $\geq$700 K, (ii) and (iv) become more important. According to ROP analysis at 700 K (see Fig. S16, ESI†), $C_{12}H_9$ non-RSR species are predicted to be formed and then rapidly consumed through second acetylene addition in early time scale, while a portion of non-RSR species isomerize to relatively stable RSR species. It has to be noted that although the amplitude of the blue dashed line (model predicted RSR species) in Fig. 5 a is comparable to red dashed line (model predicted non-RSR species), considering RSR species' high PICS (about 5 times larger than that of non-RSR species) the actual concentration of RSR species would be more than 5 times lower than that of non-RSR species. This is because the isomerization from non-RSR species to RSR species is more than an order of magnitude slower compared to non-RSR species consumption rate. At higher temperature like 800 K, fast equilibrium between non-RSR and RSR species takes place. At the same time, non-RSR species are continuously consumed through increased rate of β-scission and partially through second acetylene addition, which results in the decrease of $C_{12}H_9$ at later time scale. The experimentally observed mass signal at m/z = 153 shows reasonable agreement with the model-predicted RSR species signal as shown in Fig. 5a at later time scale. However, it is surprising that the measured m/z = 153 signal is much lower than expected at short times (<2 ms). At these times one would expect (and the model indicates) that there should be a fairly high concentration of the newly formed non-RSR adducts. This discrepancy, which might indicate $C_{12}H_9$ non-RSR adducts (N2-2, N11-2, and N8-2) have an unusually small PICS, is discussed further below.

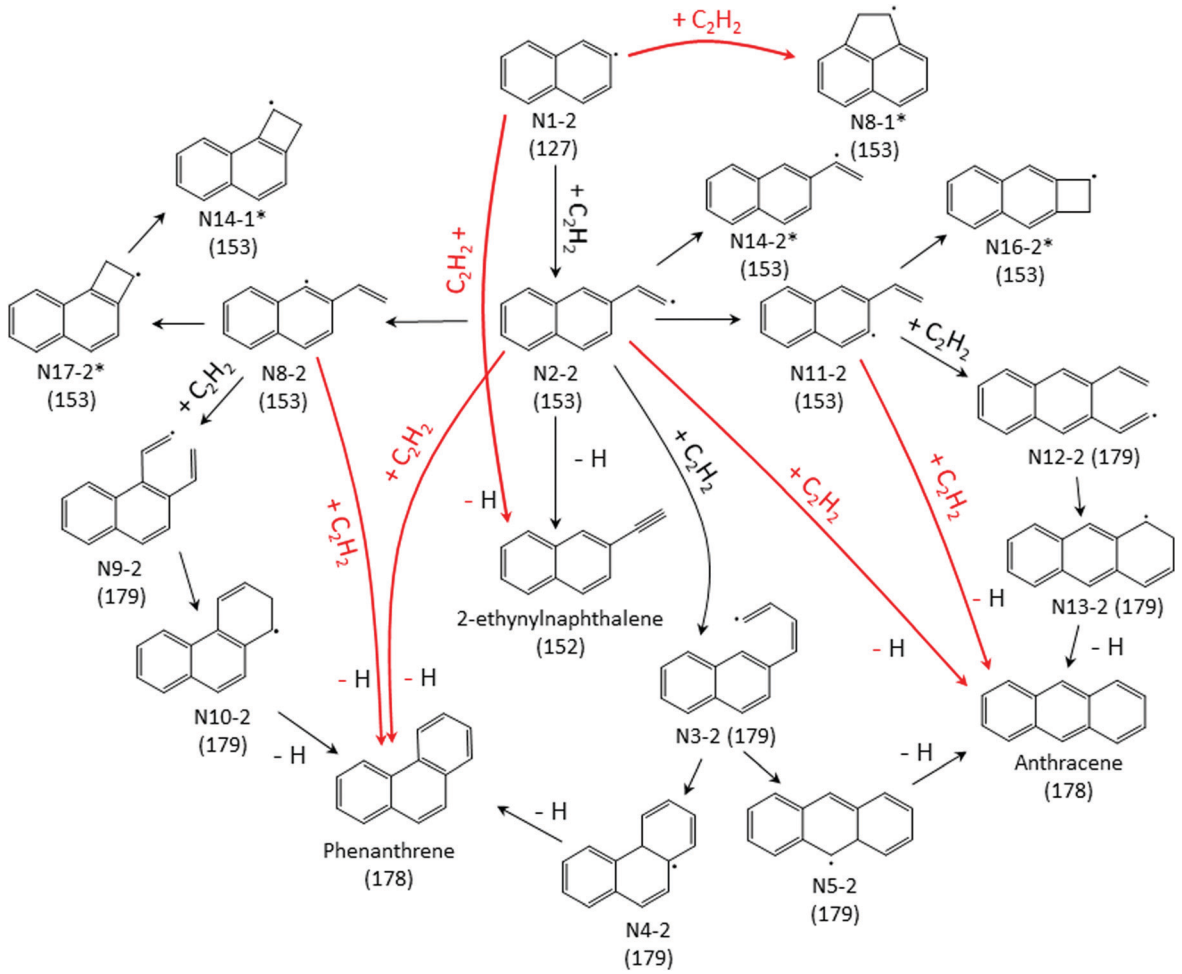

Scheme 2 Primary reaction pathways for 2-naphthalenyl + C_2H_2 predicted by the kinetic model under the experimental conditions in this work. Numbers in parentheses indicate corresponding mass-to-charge ratio of the species. The red arrows refer to well-skipping chemically-activated reaction pathways. The asterisks indicate $C_{12}H_9$ RSR species.

The product distribution formed when 2-naphthalenyl radical is mixed with C_2H_2 was measured at a total gas pressure of 15 torr and 25 torr, with the pressure increased by adding more helium. As shown in Fig. S5 (ESI†), no significant pressure-dependent product branching ratio is observed.

4.3 Discrepancies between the model predictions and the experimental data

While the main observations (*e.g.* that 1-naphthalenyl + C_2H_2 primarily forms acenaphthylene, while 2-naphthalenyl + C_2H_2 primarily forms either $C_{14}H_{10}$ PAHs or 2-ethynylnaphthalene depending on the reaction conditions) are in concord with expectations and theoretical calculations, there are also several discrepancies between the model and the experimental data, discussed in detail below.

4.3.1 1-Naphthalenyl + acetylene. In 1-naphthalenyl radical + C_2H_2 reaction, there are two main discrepancies between the model prediction and the experimental data: (i) the model always overpredicted initial formation of acenaphthylene by about a factor of 3 to 6 for reaction times 0 to 2 ms as shown in Fig. 2a–c. (ii) Unexpected observation on m/z = 178 signal. Here we explore some possible explanations for these two discrepancies.

For discrepancy (i), we consider two possible explanations: (i.1) error in the estimated PICS of acenaphthylene (54 Mb, ref. 36) or (i.2) the model overpredicts the rate coefficient for the well-skipping reaction 1-naphthalenyl radical + C_2H_2 → acenaphthylene + H. For explanation (i.1) to resolve the discrepancy, the estimated PICS of acenaphthylene in the literature would need to be about a factor of 3 too high, *i.e.* the true PICS would have to be around 18 Mb. This is possible, sometimes molecules have unexpectedly low photoionization cross-sections. The current model predicts m/z = 153 pretty well, suggesting that the uncertain estimated PICS for those isomeric radicals are not too far off. Changing the assumed PICS of acenaphthylene brings the model into much better agreement with the data (Fig. S17, ESI†), but there is still a discrepancy at long times at 800 K: experimentally the normalized m/z = 152 signal continues to grow, but the model predicts that the 152 growth should be much slower at long times right after 2 ms.

Considering alternative explanation (i.2) instead: as shown in Fig. S19a and b (ESI†), reducing the rate of the well-skipping

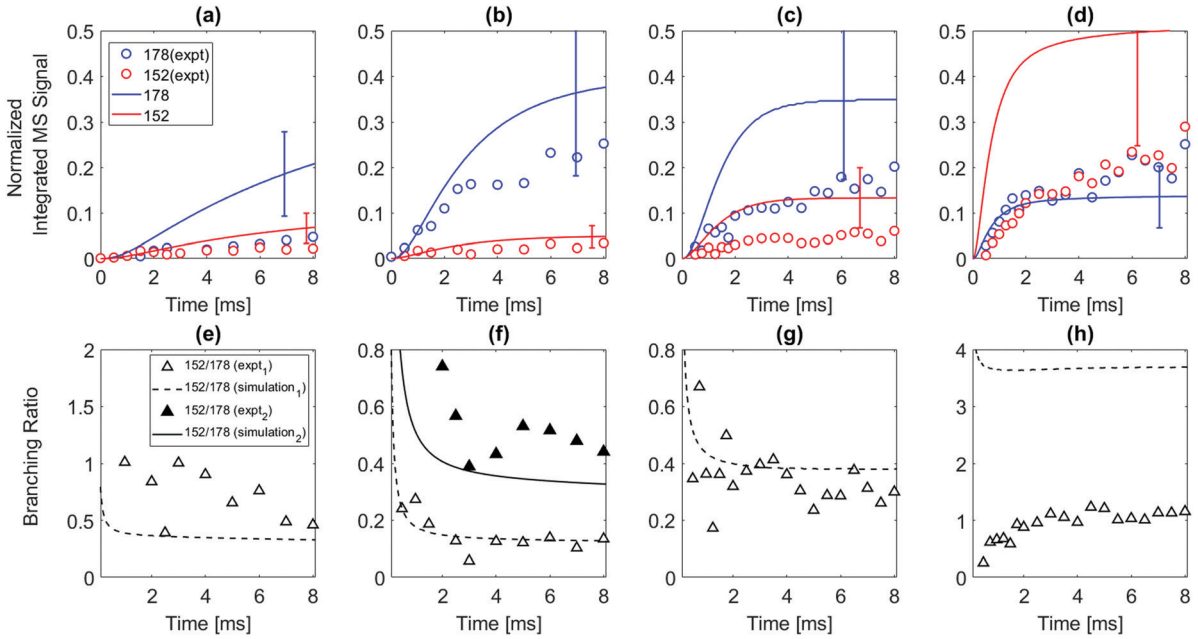

Fig. 4 (Top) Normalized time-dependent species integrated mass signals measured up to 8 ms after the photolysis pulse for the reaction of 2-naphthalenyl radical with acetylene. Red open circles indicate the signal at m/z = 152; blue open circles indicate the signal at m/z = 178; solid lines correspond to the model prediction under each experimental condition: red solid line indicates m/z = 152; blue solid line indicates m/z = 178. Uncertainty ranges of the model predictions (due to uncertainties in PICS) are shown as error bars. (bottom) The product branching ratio between m/z = 152 and m/z = 178. Black open triangle symbols indicate the experimentally observed ratio of m/z = 152 to m/z = 178; black dashed line indicates predicted ratio of m/z = 152 to m/z = 178 from the model simulation. Reactor conditions were (a) and (e) 500 K, 15 torr, initial radical concentration $[C_{10}H_7]_0 = 2.8 \times 10^{11}$ molecules per cm^3; (b) and (f) 600 K, 15 torr, initial radical concentration $[C_{10}H_7]_0 = 1.6 \times 10^{11}$ molecules per cm^3; (c) and (g) 700 K, 15 torr, initial radical concentration $[C_{10}H_7]_0 = 3.0 \times 10^{11}$ molecules per cm^3; (d) and (h) 800 K, 15 torr, initial radical concentration $[C_{10}H_7]_0 = 1.7 \times 10^{11}$ molecules per cm^3. The concentration of C_2H_2 for all the experiments was 3×10^{16} molecules per cm^3. Data and model predictions for two different acetylene concentrations are shown in figure (f) the solid line and symbols are for $[C_2H_2] = (1.0 \times 10^{16}$ molecules per cm^3).

reaction (1-naphthalenyl radical + C_2H_2 → ACN + H) by a factor of 5 significantly improves the agreement between the model prediction and the experimental data at temperatures ≤700 K. Reducing the rate of this well-skipping reaction also significantly improves agreement between the model and the experimental data on the branching ratio of m/z = 152 to 153 as shown in Fig. 2d–f, although at 800 K, the model is still over-predicting the branching ratio of m/z = 152 to 153 at longer timescale. A factor of 5 error in the computed rate coefficient is not impossible; it could be due to errors in the calculated reaction barriers or due to the Modified Strong Collision approximation that was used to calculate the pressure-dependent rate coefficients in Chu *et al.*[22] Previous work by Allen *et al.*[39] showed that this approximation often introduces errors of about a factor of 3 in calculated rate coefficients for chemically-activated reactions, so a factor of 5 error would not be surprising. However, explanation (i.2) is not sufficient to fully resolve the discrepancy: at 800 K, the adjusted model still over-predicts the rate of chemically-activated formation of acenaphthylene. But adjusting this one rate coefficient significantly improves the predicted product branching ratio between 152 and 153 in every experiment.

We conclude it is likely that discrepancy (i) is mainly due to combined effects of both uncertainties in PICS of acenaphthylene and errors in the well-skipping reaction's rate coefficient.

Discrepancy (ii) is the unexpected appearance of m/z = 178 signal from the experiments using 1-iodonaphthalene as a precursor at longer times, as can be observed in Fig. 2. Although m/z = 178 species such as phenanthrene and anthracene are predicted (and observed) to be major products from 2-naphthalenyl, none of the theoretical studies predict significant m/z = 178 formation from 1-naphthalenyl. However, m/z = 178 signals were not observed from experiments that use 1-bromonaphthalene as a precursor, which indicates that m/z = 178 peak is a result of iodine-dependent secondary chemistry. For more detailed discussion of this unexpected peak, which we believe is C_4H_3I, see the ESI.†

4.3.2 2-Naphthalenyl + acetylene. In the 2-naphthalenyl + C_2H_2 experiments, there are three main discrepancies: (iii) quantitative discrepancy between model predictions and experimental data on m/z = 152 and 178 at temperatures other than 600 K; (iv) experimentally observed m/z = 178 signal still increasing at longer time scale (>4 ms) at 700 and 800 K (Fig. 4c and d); and, (v) discrepancy in the m/z = 153 intermediate at short times (Fig. 5a).

Discrepancy (iii): while the model and experiment are qualitatively in concord for the 2-naphthalenyl + C_2H_2 case, there are several quantitative discrepancies between the model predictions and measurements of the major products at m/z = 152 and m/z = 178 at certain temperatures. For example, at 500 and 700 K, the model over-predicts the formation of m/z = 178 about a factor of 3–4, and over-predicts the formation of m/z = 152 about a factor of 2–3. At 800 K, the model predicts the

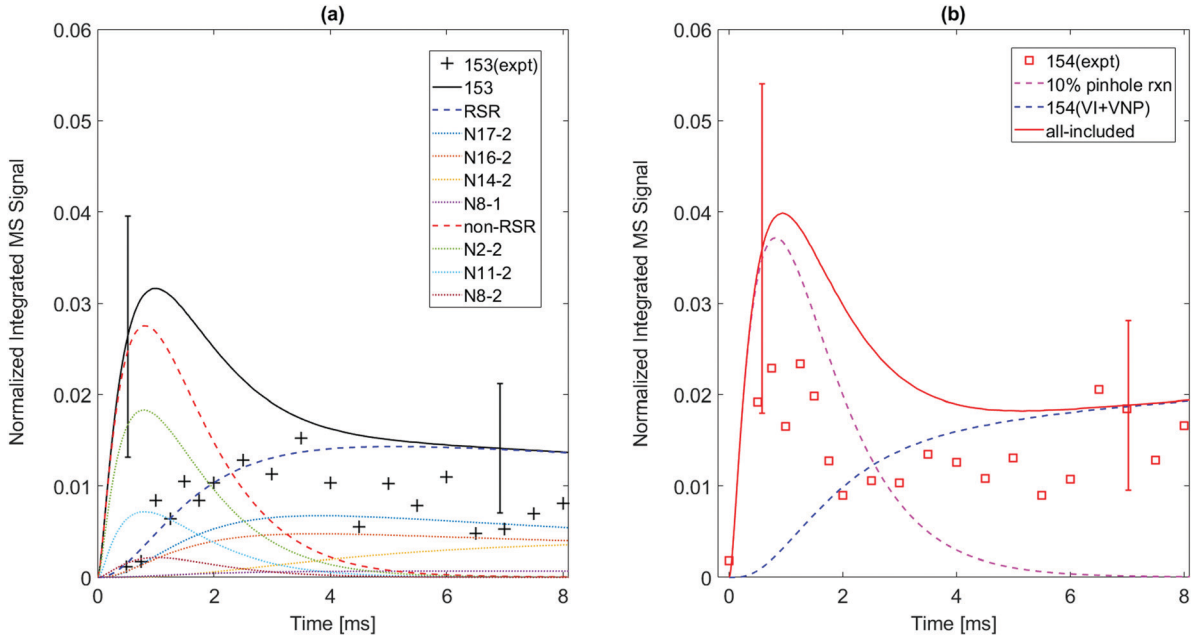

Fig. 5 Model predictions (solid) *vs.* experimental data for m/z = 153 and m/z = 154 formed when 2-naphthalenyl radical is formed in an C_2H_2/He mixture at 700 K, P = 15 torr. Uncertainties in the predictions due to estimated PICS are shown as error bars. (a) Several isomeric $C_{12}H_9$ radicals are predicted to contribute significantly to the m/z = 153 signal, see Scheme 2. Most of the observed m/z = 153 signal is from long-lived resonantly stabilized radicals (N17-2, N16-2, N14-2, N8-1); their sum is the blue-dashed RSR curve. The model over-predicts signals from short-lived reactive non-stabilized m/z = 153 radicals (N2-2, N11-3, N8-2); their sum is the red-dashed "non-RSR" curve. This discrepancy may be due to low PICS of those radicals or fragmentation of their parent ions. (b) The early peak in the m/z = 154 signal (magenta dashed curve) is attributed to products from the m/z = 153 non-RSR formed in the pinhole (see text). The blue-dashed curve is the model's prediction of signal from stable m/z = 154 species (vinyl iodide, vinyl naphthalene) formed by slower secondary reaction sequences.

formation of m/z = 178 well up to 3 ms, but under-estimates it at longer time scale. In the case of m/z = 152 formation at 800 K, the model over-estimates the formation of m/z = 152 about a factor of 2–3 over time. One of course would not expect the model predictions to perfectly match the experimental data even if we knew the PICS to perfect accuracy, since the rate coefficients used in the model are somewhat uncertain. Here we consider whether modest variations in some of the rate coefficients, within their uncertainties, would be enough to resolve these quantitative discrepancies.

We computed the sensitivity of the main m/z = 152 and 178 species to all of the rate coefficients in the model (Fig. S24 and S25, ESI†). The most sensitive five reactions are

$$\text{N2-2} + C_2H_2 \rightarrow \text{Phenanthrene} + \text{H} \quad (5)$$

$$\text{N2-2} + C_2H_2 \rightarrow \text{Anthracene} + \text{H} \quad (6)$$

$$\text{N11-2} + C_2H_2 \rightarrow \text{Anthracene} + \text{H} \quad (7)$$

$$\text{N2-2} \rightarrow \text{2-ethynylnaphthalene} + \text{H} \quad (8)$$

$$\text{N2-2} + \text{I} \rightarrow \text{2-ethynylnaphthalene} + \text{HI} \quad (9)$$

They each have normalized sensitivities $\frac{d(\ln C_n)}{d(k_i)}$ with magnitudes in the range of 0.3–0.8. The sensitivities for different products have different signs, and their magnitudes vary with temperature. There is no way to modify just one of the rate coefficients to resolve the discrepancies in m/z = 152 and m/z = 178 at all the temperatures. However, we find that there are combinations of reasonable modifications within the expected uncertainties of the rate coefficients that mostly resolve the discrepancies. For example, if one reduces I atom involved disproportionation rate coefficient (reaction (9)) by half, reduces β-scission rate coefficient (reaction (8)) by a factor of 5, and reduces well-skipping reaction rate coefficient (reaction (5)) by a factor of 5, the model is in pretty good agreement with the m/z = 152 and m/z = 178 data (see Fig. S26, ESI†).

We note that this by no means a firm determination of the rate coefficients for these 5 reactions – there are too many model parameters and too few experimental data to allow a unique determination of the model parameters (and keep in mind that there are a large number of uncertain PICS) and several other moderately sensitive rate coefficients in the model, not just these 5 most sensitive reactions. However, the fact that modest adjustment of a few rate coefficients can bring the model into much better agreement suggests that quantitative discrepancy (iii) is not indicating a fundamental problem, but is more a reflection of our imperfect knowledge of the values of the model parameters.

Discrepancy (iv): while small adjustment of the 5 most sensitive rate coefficients can resolve most of discrepancies for m/z = 152 and m/z = 178, it doesn't resolve the discrepancy between the model and the data on m/z = 178 at 700 and 800 K at long times (>4 ms). According to our model, the $C_{14}H_{10}$ formation chemistry should essentially be over by this time, so

the model trajectory is quite flat at long times. We hypothesize that the additional 178 signal growing in at long times (Fig. 5c and d) is not $C_{14}H_{10}$, but instead is C_4H_3I formed by some unknown secondary iodine chemistry, as is seen in the 1-naphthalenyl + C_2H_2 experiments (see Section 4.3.1). To test this hypothesis, we repeated the 2-naphthalenyl + C_2H_2 experiment using 2-bromonaphthalene instead of 2-iodonaphthalene as the precursor. The results are shown in Fig. S21b and S27, and discussed more in the ESI.† In the iodine-free system, we still observe m/z = 178 formation at short times from the expected hydrocarbon chemistry (*e.g.* reactions (5)–(7) above). But in the absence of any source of iodine, we no longer see the extra m/z = 178 growth at long times, consistent with the hypothesis.

Discrepancy (v): the model prediction for m/z = 153 at 700 K matched the experimental data fairly well for times >3 ms, but predicted a strong signal at shorter times which was not observed. As previously mentioned in Section 4.2.2, this could happen if the $C_{12}H_9$ non-RSR species had an unusually small PICS, while their RSR isomers have normal PICS. According to the model, the very reactive non-RSR $C_{12}H_9$ species are formed first but are quickly consumed, while the stabler RSR isomers have long lifetimes. This hypothesis is consistent with the experimental observation in Fig. 5a. Similar data on m/z = 153 at other experimental conditions are presented in the ESI.† As you can see from Fig. 5a, the model predicts that most of the m/z = 153 signal at early times (<3 ms) is due to $C_{12}H_9$ non-RSR species, where there is a model-data discrepancy (since the model assumes a normal PICS for all non-RSR radicals). However, after 3 ms, the model predicts most of the m/z = 153 signal is due to $C_{12}H_9$ RSR species, and at those times the model shows reasonable agreement with experimentally observed m/z = 153 signals. So, we conclude it is likely that discrepancy (v) is mainly due to the unusually small PICS of $C_{12}H_9$ non-RSR species. The unexpectedly low PICS is unfortunate, since it means we cannot directly observe time-dependent behavior of $C_{12}H_9$ non-RSR species which are predicted to be important at early times (<3 ms). However, we can observe the time-behavior of $C_{12}H_9$ non-RSR species indirectly, taking advantage of a side-reaction discussed in the following section.

4.4 The effect of side reactions

The chemical kinetic analysis of the time-dependent product signal is affected by side reactions that perturb measured signal intensities. The side reactions and how they are addressed are described in the following section.

4.4.1 Side reactions at the reactor pinhole. As shown in Fig. 5b for 2-naphthalenyl + C_2H_2, a significant m/z = 154 signal intensity is observed after photolysis of 2-iodonaphthalene in the presence of C_2H_2. This signal is attributed primarily to vinylnaphthalene (VNP, $C_{12}H_{10}$) and vinyliodide (VI, C_2H_3I). In the model prediction, vinylnaphthalene formation is due to secondary recombination of $C_{12}H_9$ isomers with a H-atom, and C_2H_3I formation is due to secondary recombination of I atoms and C_2H_3 after the secondary $C_2H_2 + H \rightarrow C_2H_3$ reaction. However, as shown in Fig. 5b, the linear combination of the computed signal intensities for VI and VNP (C_2H_3I and $C_{12}H_{10}$, blue dashed line) does not agree well with experimental m/z 154 signal intensity before 2 ms. There is an extra peak in the m/z = 154 signal at early times (<2 ms). Additionally, when 2-iodonaphthalene is photolyzed without added acetylene, the m/z = 128 signal ($C_{10}H_8$ and HI) increases at early reaction times (up to 2 ms) before decreasing and then increasing again (Fig. S3d in ESI†) – qualitatively similar to the shape of the m/z = 154 time profile in Fig. 5b. To rationalize the discrepancy in computed and experimental m/z = 154 signal intensity in Fig. 5b, we consider a wall reaction where labile H-atoms are added to $C_{12}H_9$ radicals to generate $C_{12}H_{10}$ isomers.

Wall reactions are typically assumed to occur before the reactants and products reach the pinhole, and thus would influence the chemistry inside the reactor by acting as an additional sink for radicals. As the concentration of radicals decreases due to reactions with the wall, the stable product formed by the wall reaction is expected to gradually increase and then reach a plateau.[24] However, the time behavior of both m/z = 154 and m/z = 128 in this study differs from the expected behavior for typical wall reaction: the signal rises and peaks at early reaction times, decreases with a time constant of 1–2 ms, and then increases at longer time scale again before stabilizing. This is not consistent with a wall reaction forming a stable product. (Note m/z = 154 is a stable closed shell hydrocarbon $C_{12}H_{10}$ which should have a long lifetime at our reaction conditions.) Hence, we hypothesize the observed behavior in Fig. 5b results from wall reactions within the pinhole in the reactor wall – referred to here as ''pinhole reactions'', distinct from the typical wall reaction described above. The stable products formed in the pinhole reactions such as $C_{12}H_{10}$ rapidly flow out of the pinhole, and they do not diffuse back into the main reactor volume. Note the concentration of the stable m/z = 154 species in the main reactor volume is clearly much lower than it is inside the pinhole, otherwise the m/z = 154 signal would not decrease so rapidly.

We assume that the observed m/z = 154 signal shown in Fig. 5b can be attributed to some fraction of $C_{12}H_9$ radicals (m/z = 153) undergoing pinhole reactions. To estimate the effect of pinhole reactions on the kinetic model, we analyze the predicted concentrations of m/z = 153 products and compare their time behavior to the experimentally observed m/z = 154 signal. An agreeable fit is obtained by assuming that $C_{12}H_9$ resonance-stabilized radical (RSR) isomers leave the reactor without undergoing a pinhole reaction, while 10% of the much more reactive non-resonance-stabilized radicals ($C_{12}H_9$ non-RSR species) capture H atom at the pinhole and produce the signal at m/z = 154. This assumption is reasonable since RSR species are much less reactive than non-RSR species.[15] The pinhole reaction product is assumed to be vinylnaphthalene ($C_{12}H_{10}$) under all tested experimental conditions (500–800 K; 15 and 25 torr) for the 2-naphthalenyl + C_2H_2 chemical mechanism (other conditions can be found in ESI†). As shown in Fig. 5b, the computed m/z = 154 signal intensity that accounts for pinhole reactions of 10% $C_{12}H_9$ non-RSRs can explain this early peak of m/z = 154 at around 1 ms. In the case

of 1-naphthalenyl + C_2H_2, this behavior is not observed and easily rationalized because the m/z = 153 is predicted to be predominantly N8-1, a RSR.

This pinhole reaction assumption can be used to infer the behavior of non-RSR species at early reaction times. The initial increase of m/z = 154 intensity is attributed to reactions of the $C_{12}H_9$ non-RSRs in the pinhole when their concentration is high. Soon, $C_{12}H_9$ non-RSR concentration decreases through β-scission to form 2-ethynylnapthalene, or second acetylene addition to form phenanthrene or anthracene, consistent with the decrease of m/z = 154 as shown in Fig. 5b. The m/z = 154 signal seen at longer times ($\geq$3 ms) after the $C_{12}H_9$ non-RSR concentration has decayed, is primarily due to products of secondary reactions occurring in the main reactor volume: recombination of $C_{12}H_9$ RSR isomers with H-atom and the recombination $C_2H_3 + I \rightarrow C_2H_3I$.

4.4.2 C_2H_3 + C_2H_2 side reaction. As mentioned in Section 4.1, we observe evidence for the reaction of vinyl radicals (C_2H_3) with C_2H_2 and this might affect kinetic measurement for the naphthalenyl radical + C_2H_2 reaction. According to Smith *et al.*,[28] C_2H_3 + C_2H_2 reaction leads to butadienyl radicals (C_4H_5) and vinylacetylene (C_4H_4) with subsequent second acetylene addition to C_4H_5 leads to C_6H_7 and C_6H_6. These reactions are included within the model and predicted to occur under the experimental conditions. The comparison to experimental data is included in the ESI.† While these side reactions are indeed occurring, based on sensitivity analysis, we conclude that they reaction have a negligible impact on the naphthalenyl radical + C_2H_2 reactions of interest.

4.4.3 I atom side reactions. Side reactions caused by I atoms are also observed in the experiments reported here. The I atom recombination with vinyl radicals (C_2H_3) and C_4H_5 produces C_2H_3I (m/z = 154) and C_4H_5I (m/z = 180), respectively. These I atom recombination reactions have a negligible impact on the measured kinetic behavior of the naphthalenyl + C_2H_2 reactions – consistent with the kinetic model. However, the disproportionation reaction I + $C_{12}H_9 \rightarrow$ ACN + HI becomes non-negligible after 5 ms, accounting for up to 10% of acenaphthylene predicted in the model simulation for 1-naphthalenyl + C_2H_2. In the 2-naphthalenyl + C_2H_2 case, removal of the H-atom by I in this way accounts for more than 80% of the 2-ethynylnaphthalene formed at reactor temperatures $\leq$600 K. However, at temperatures $\geq$700 K this reaction is not competitive against β-scission of N2-2 to form 2-ethynylnaphthalene and H atom.

4.5 Comparison with previous experimental study of the naphthalenyl + C_2H_2 reaction

There has been one previous fairly direct experiment that selectively formed 2-naphthalenyl radical in the presence of C_2H_2.[21] In sharp contrast with the present work, the prior experiment failed to detect any $C_{14}H_{10}$ (*e.g.* phenanthrene, anthracene) formation, but we observe $C_{14}H_{10}$ (m/z = 178) as one of the major products.

The yield of $C_{14}H_{10}$ is expected to strongly depend on several aspects of the reaction conditions: radical concentration, temperature, acetylene concentration, reaction time, and pressure. High radical concentrations are needed to drive the high-temperature Frenklach mechanism.[7,8,32] The low-temperature Bittner–Howard mechanism[9] relies on pressure to trap the initial radical adduct and a high acetylene concentration to react with that radical before it beta-scissions.

In the prior experiment, the 2-naphthalenyl radical was generated by pyrolysis of 2-iodonaphthalene, but in the present work the radical was generated by photolysis. (Also in the present work we did a control experiment using 2-bromonaphthalene as the radical precursor instead of 2-iodonaphthalene.) Photolysis generates approximately the same radical concentration in every experiment, mostly set by the number of photons in the flash, but in the pyrolysis experiment the radical concentration depends strongly on the temperature. As a consequence, the pyrolysis experiments become very challenging at low temperature, since only very small concentrations of radicals and products are generated. Lifshitz *et al.*[29] reported the rate coefficient of 1-iodonaphthalene dissociation at 1000 K to be 4.84 s^{-1} at 1000 K. Assuming that the dissociation of 2-iodonaphthalene has a similar rate, this implies $<$0.1% of it dissociated to form radicals during the 0.1 ms timescale[40–42] of Parker's experiments. Parker *et al.*[21] say that they did not detect $C_{14}H_{10}$ "from room temperature to 1500 K". But since the pyrolysis rate coefficient drops very rapidly with temperature, at room temperature the radical formation rate in Parker *et al.*'s[21] apparatus must have been near zero. Because of the very small radical concentrations produced pyrolytically at low temperatures, we doubt that Parker *et al.*[21] had sufficient signal-to-noise to measure products of radical reactions in the 500–800 K range of the experiments reported here. The lowest temperature data published by Parker *et al.*[21] was measured at 1000 K.

Although one would expect problems at lower temperatures, at 1000 K, Parker *et al.*'s[21] pyrolysis experiment definitely had enough sensitivity to detect $C_{14}H_{10}$ if it was a significant minor product. Indeed, in earlier work in the same apparatus, Parker *et al.*[14] observed the analogous reaction of phenyl radical adding two C_2H_2's to form naphthalene, and measured that about 5% of the phenyl radicals followed this path rather than stopping after adding one C_2H_2. One would expect 2-naphthalenyl radical would behave similarly at 1000 K, with a few percent of the initial adduct adding a second C_2H_2 to form $C_{14}H_{10}$. We see both reaction pathways as being competitive at our conditions at 800 K (*e.g.* see Fig. 4d). The yield of $C_{14}H_{10}$ is expected to drop with temperature, but it remains an unresolved mystery why it apparently dropped very sharply from 800 to 1000 K, so $C_{14}H_{10}$ could not be detected at all in the higher temperature experiments. Eyeballing the Parker *et al.*[21] data, it appears their experiment sets an upper bound on m/z = 178 signal of about 1% of their measured m/z = 152 ($C_{12}H_8$) product at 1000 K.

In contrast, the current measurements on 1-naphthalenyl + C_2H_2 are in reasonable concord with the prior experiments by Parker *et al.*[21] and also by Lifshitz *et al.*[29] The experiments and the models all agree that over a broad range of reaction

conditions the major stable product from 1-napthalenyl + C_2H_2 is $C_{12}H_8$, primarily the isomers acenaphthalene and 1-ethynylnaphthalene.

5 Conclusions

Modelers expect 2-naphthalenyl radical will sequentially add 2 C_2H_2's in a HACA process to form the 3-ring $C_{14}H_{10}$ aromatics phenanthrene or anthracene, either *via* a stable intermediate 2-ethynylnaphthalene (the Frenklach mechanism[7,8,32]) at high temperature or *via* a reactive $C_{12}H_9$ radical adduct (*e.g.* the Bittner–Howard mechanism[9] or the modified Frenklach mechanism[17,18]) at lower temperatures. There have been many modeling studies on this system over several decades, most recently by Chu *et al.*[22] Phenanthrene and anthracene are often observed as products in real-world systems with high concentrations of acetylene and aromatics. However, this observation does not prove the hypothesized reaction mechanisms since many reactions are occurring in those systems, and there are usually no attempt to measure the naphthalenyl radicals. In the present work, for the first time, formation of $C_{14}H_{10}$ as a major product was observed in a direct experiment starting with 2-naphthalenyl radical, more or less consistent with model predictions.

Here we report the first direct measurement of the time-dependent kinetic behavior and product distributions for the reactions of 1-naphthalenyl and 2-naphthalenyl radicals with C_2H_2, using VUV-PI-TOF-MS (PI energy = 10.49 eV) from 500 to 800 K and 15 to 50 torr. The reaction of 1-naphthalenyl radical with C_2H_2 led to product signal at m/z = 153, corresponding to a $C_{12}H_9$ radical intermediate, N8-1 in the model prediction; m/z = 152, corresponding to stable acenaphthylene ($C_{12}H_8$) in the model prediction; and m/z = 178, which was not expected in the model prediction, likely C_4H_3I based on the result from the control experiment. In the reaction of 2-naphthalenyl radical with C_2H_2, the main products are m/z = 152, corresponding to 2-ethynylnaphthalene ($C_{12}H_8$) in the model prediction; and m/z = 178, corresponding to phenanthrene and anthracene ($C_{14}H_{10}$) in the model prediction. Other products were observed at m/z = 153, corresponding to isomeric ($C_{12}H_9$) radicals in the model prediction; and m/z = 154, corresponding to the product formed after non-resonance stabilized radical isomers captured H-atom on the walls of the pinhole or at longer timescales from secondary chemistry ($C_{12}H_{10}$) as well as C_2H_3I formed from side reactions involving I atom. The experiments were compared with a model of the temperature-dependent kinetics constructed using *ab initio* quantum calculations by Chu *et al.*[22] The model qualitatively described the 1-naphthalenyl radical + C_2H_2 temperature-dependent product branching ratio, but overpredicted the rate of production of m/z = 152 at every experimental condition. Furthermore, the model couldn't account for the formation of m/z = 178 (C_4H_3I) at temperature above 700 K. For 2-naphthalenyl radical + C_2H_2, the model predicted the product branching ratio between m/z = 152 and 178 fairly well at the temperature between 600 and 700 K; underpredicted at 500 K; and overpredicted at 800 K. However, the model captured qualitative temperature dependent behavior of product branching ratio for both reaction systems (1-naphthalenyl + C_2H_2 and 2-naphthalenyl + C_2H_2). As discussed in some detail here, inaccurate model parameters, errors in PICS, and mechanism truncation error may be responsible for the discrepancies between the model prediction and the experimental data. This work provides direct experimental evidence for formation of significant yields of tricyclic $C_{14}H_{10}$ PAHs from sequential addition of 2 acetylene molecules to 2-naphthalenyl radicals, in contrast with a recent report that suggested $C_{14}H_{10}$ products are not formed below 1500 K.

Conflicts of interest

There are no conflicts to declare.

Acknowledgements

The authors gratefully acknowledge SABIC and the FAA for financial support. We gratefully acknowledge Matt Johnson's help with RMG and RMS usage. We thank Prof. Alexander Mebel and Dr Istvan Lengyel for providing detailed theoretical calculations used to construct the kinetic model, and Yoshinaga Kosuke for H-NMR analysis. We thank Dr Musahid Ahmed and Dr Wenchao Lu for providing mass-spec data of supplementary 2-iodonaphthalene + C_2H_2 experiment at various photon energy.

Notes and references

1 M. P. Bernstein, S. A. Sandford, L. J. Allamandola, J. S. Gillette and S. J. Clemett, *Science*, 1999, **283**, 1135–1138.
2 G. Grimmer, *Environmental Carcinogens: Polycyclic Aromatic Hydrocarbons*, CRC Press, 1983.
3 H. Richter and J. Howard, *Prog. Energy Combust. Sci.*, 2000, **26**, 565–608.
4 V. V. Kislov, A. I. Sadovnikov and A. M. Mebel, *J. Phys. Chem. A*, 2013, **117**, 4794–4816.
5 A. M. Mebel, Y. Georgievskii, A. W. Jasper and S. J. Klippenstein, *Proc. Combust. Inst.*, 2017, **36**, 919–926.
6 T.-C. Chu, PhD thesis, Massachusetts Institute of Technology, 2020.
7 M. Frenklach and H. Wang, *Symp. (Int.) Combust., [Proc.]*, 1991, **23**, 1559–1566.
8 M. Frenklach, D. W. Clary, W. C. Gardiner and S. E. Stein, *Symp. (Int.) Combust., [Proc.]*, 1985, **20**, 887–901.
9 J. D. Bittner and J. B. Howard, *Symp. Combust. Proc.*, 1981, **18**, 1105–1116.
10 M. Frenklach, R. I. Singh and A. M. Mebel, *Proc. Combust. Inst.*, 2019, **37**(1), 969–976.
11 A. Fahr and S. Stein, *Symp. (Int.) Combust., [Proc.]*, 1989, **22**, 1023–1029.
12 T. Yu and M. C. Lin, *J. Am. Chem. Soc.*, 1993, **115**, 4371–4372.
13 T. Yu, M. C. Lin and C. F. Melius, *Int. J. Chem. Kinet.*, 1994, **26**, 1095–1104.

14 D. S. N. Parker, R. I. Kaiser, T. P. Troy and M. Ahmed, *Angew. Chem.*, 2014, **53**, 7740–7744.
15 T.-C. Chu, Z. J. Buras, M. C. Smith, A. B. Uwagwu and W. H. Green, *Phys. Chem. Chem. Phys.*, 2019, **21**, 22248–22258.
16 M. Frenklach and A. M. Mebel, *Phys. Chem. Chem. Phys.*, 2020, **22**, 5314–5331.
17 N. W. Moriarty, N. J. Brown and M. Frenklach, *J. Phys. Chem. A*, 1999, **103**, 7127–7135.
18 M. Frenklach, N. W. Moriarty and N. J. A. Brown, *Symp. Combust. Proc.*, 1998, **27**, 1655–1661.
19 A. Lifshitz, C. Tamburu and F. Dubnikova, *J. Phys. Chem. A*, 2009, **113**, 10446–10451.
20 J. Park, H. M. T. Nguyen, Z. F. Xu and M. C. Lin, *J. Phys. Chem. A*, 2009, **113**, 12199–12206.
21 D. S. N. Parker, R. I. Kaiser, B. Bandyopadhyay, O. Kostko, T. P. Troy and M. Ahmed, *Angew. Chem.*, 2015, **54**, 5421–5424.
22 T.-C. Chu, M. C. Smith, J. Yang, M. Liu and W. H. Green, *Int. J. Chem. Kinet.*, 2020, **52**, 752–768.
23 J. E. Middaugh, Z. J. Buras, M. Matrat, T.-C. Chu, Y.-S. Kim, I. M. Alecu, A. K. Vasiliou, C. F. Goldsmith and W. H. Green, *Rev. Sci. Instrum.*, 2018, **89**, 074102.
24 Z. J. Buras, T.-C. Chu, A. Jamal, N. W. Yee, J. E. Middaugh and W. H. Green, *Phys. Chem. Chem. Phys.*, 2018, **20**, 13191–13214.
25 S. E. Van Bramer and M. V. Johnston, *Appl. Spectrosc.*, 1992, **46**, 255–261.
26 M. P. McCann, C. H. Chen and M. G. Payne, *J. Chem. Phys.*, 1988, **89**, 5429–5441.
27 Z. J. Buras, PhD thesis, Massachusetts Institute of Technology, 2018.
28 M. C. Smith, G. Zhu, Z. J. Buras, T.-C. Chu, J. Yang and W. H. Green, *J. Phys. Chem. A*, 2020, **124**, 2871–2884.
29 A. Lifshitz, C. Tamburu and F. Dubnikova, *J. Phys. Chem. A*, 2008, **112**, 925–933.
30 C. W. Gao, J. W. Allen, W. H. Green and R. H. West, *Comput. Phys. Commun.*, 2016, **203**, 212–225.
31 M. S. Johnson, H. Pang, X. Dong and W. H. Green, Reaction Mechanism Simulator, https://github.com/ReactionMechanismGenerator/ReactionMechanismSimulator.jl.
32 H. Wang and M. Frenklach, *J. Phys. Chem.*, 1994, **98**, 11465–11489.
33 J. C. Robinson, N. E. Sveum and D. M. Neumark, *Chem. Phys. Lett.*, 2004, **383**, 601–605.
34 H. Xu and S. T. Pratt, *J. Chem. Phys.*, 2013, **139**, 214310.
35 Z. Zhou, M. Xie, Z. Wang and F. Qi, *Rapid Commun. Mass Spectrom.*, 2009, **23**, 3994–4002.
36 Y. Y. Li, J. Z. Yang and Z. J. Cheng, Edited by JiuZhong Yang and Combustion Team, Photonionization Cross Section Database (Version 2.0), 2017, http://flame.nsrl.ustc.edu.cn/database/.
37 G. Malloci, G. Mulas and C. Joblin, *Astron. Astrophys.*, 2004, **426**, 105–117.
38 H. W. Jochims, H. Baumgartel and S. Leach, *Astron. Astrophys.*, 1996, **314**, 1003–1009.
39 J. W. Allen, C. F. Goldsmith and W. H. Green, *Phys. Chem. Chem. Phys.*, 2012, **14**, 1131–1155.
40 P. Chen, S. D. Colson, W. A. Chupka and J. A. Berson, *J. Phys. Chem.*, 1986, **90**, 2319–2321.
41 P. Chen, J. B. Pallix, W. A. Chupka and S. D. Colson, *J. Chem. Phys.*, 1986, **86**, 516–520.
42 Q. Guan, K. N. Urness, T. K. Ormond, D. E. David, G. B. Ellison and J. W. Daily, *Int. Rev. Phys. Chem.*, 2014, **33**, 447–487.